VOL. 14, NO. 19, OCTOBER 2019 ISSN 1819-6608
ARPN Journal of Engineering and Applied Sciences

www.arpnjournals.com

PRODUCTION OF SPINEL FORSTERITE REFRACTORIES USING SHEARED SERPENTINIZED ULTRAMAFIC ROCKS, UM SELEIMAT, EGYPT

W. Abdelwahab, H. Mekky, A. Khalil and Z. Belal
Geological Sciences Department, National Research Centre, El-Buhouth St., Dokki, Cairo, Egypt
E-Mail: wa.wahab@nrc.sci.eg

ABSTRACT

The present work aims at assessment and utilization of some Egyptian Sheared serpentinized ultramafic rocks, from Um Seleimat ophiolites at Central Eastern Desert (CED), for producing refractory forsterite and spinel forsterite composites. Generally, Egyptian serpentinized ultramafic rocks occur in two types, massive and sheared serpentinites. To perform the study aim, two batches were designed on base of stiochiometrical calculations of specific proportions of "used magnesia" and/or "calcined bauxite" in addition to the serpentinized ultramafic rocks and fired at 1500°C for two hours to form forsterite and spinel forsterite. Chemical and mineralogical studies were carried out for the starting materials, while mineralogical composition, scanning electron microscope, EDAX as well as physical parameters and thermo-mechanical properties, are done for the fired batches. In addition, the compressive strength as well as the refractoriness under load was done. The study results indicated that forsterite and spinel composites were produced from serpentinites by adding a calculated amount of used magnesia and/or calcined bauxite mixed to the studied sheared serpentinized rocks. Based on the previously measured physical as well as thermo-mechanical properties of the synthetic composites, it is recommended to be applied as refractory materials in lining of permanent layer of iron and steel ladles and the brick network in the heat exchangers of glass furnaces.

Keywords: ultramafic rocks, serpentinite, Um seleimat, forsterite, spinel, refractories, refractoriness under load.

1. INTRODUCTION

The excellent refractoriness of forsterite means withstand the high temperature even at high load without noticeable changing in its physical and chemical properties. As a high-grade refractory, the volume stability, high strength, low thermal expansion, and excellent abrasion and erosion resistance characterize the forsterite. corrosion and mechanical as well as thermal shocks [1, 2]. Forsterite is used in the lining of slag belt of steel ladles and steel casting nozzles, stopper tubes, hearth of soaking pits, burning zones of cement rotary kilns, etc. It is also important for checker brick applications and allow raising the checker temperature to 1400°C, which is much above than that of conventionally used aluminosilicate refractories [3, 4].

Mineralogically, forsterite (Mg_2SiO_4) is magnesium - rich olivine, classified as an orthosilicate mineral, and occurs as a part of the isomorphous chain with Fayalite (Fe_2SiO_4) in the olivine cycle. The natural olivine is a complete solid solution of forsterite and fayalite, varies in colour from yellow to olive green, and has a melting point around 1750°C (for commonly available minerals). Its specific gravity varies in the range of 3.27 to 3.37 and hardness varies from 6.5 to 7 in Mohs' scale [7, 8]. Regarding forsterite, it melts at 1890°C, while fayalite at 1205°C and thus the melting point of usual mineral is lower if there is solid solution between them[5,6]. The excellent insulation properties of forsterite result for the comparatively high temperature creep resistance and low thermal conductivity.

The natural Mg-rich olivine crystallizes from magma that is rich in magnesium and low in silica, forming mafic / ultramafic rocks, which mostly represent the ocean floor. The ultramafic rocks more enriched in olivine such as Peridotite, harzburgites, lherzolitesand, and dunite, can be left after the extraction of magma. The rate of synthetic forsterite hydration determined experimentally by Martin and Fyfe, 1970 [9] has become over the years the reference data set to parameterize serpentinization kinetics in olivine -host rocks metamorphic transformation models, and the nature of the serpentine mineral product depended on the initial olivine grain size. The recent kinetic data make the range of olivine grain sizes and reaction temperatures are relevant to the serpentinization of olivine in the oceanic crust in so far as water is available. Initially, the complete sequence of ophiolite complexes, similar to that of the ocean floor, is composed, from the top to the base, of pillow lavas, sheeted dikes, layered gabbros, and upper mantle peridotites. Mg-rich olivine- host rocks are mostly occurred within the ophiolite sequence [10, 11, 12]. The Neoproterozoic ophiolites in the CED of Egypt (690 to 890 Ma) are a part of the Arabian-Nubian Shield (ANS) that was formed during the tectonic evolution (900-550Ma) of the Pan-African Orogen. The ANS ophiolites at CED, as older ophiolite complexes, are severely fragmented and dismembered. They are subjected to complicated post-magmatic histories including: intense serpentinization, regional deformation, and contact metamorphism that destroyed many of their primary characteristics. Therefore, there is no natural forsterite mining work rather than some of the finest gem-quality olivine has been obtained from a body of mantle rocks on Zabargad Island in the Red Sea [13,14,15,16,17,18,19,20,21,22].

There are two types of procedures have been performed to practice forsterite ceramics, the first one is

based on the sol-gel technique, which is considered a high cost method, while the second is a solid-state reaction - based [23, 24]. The later produces forsterite for large-scale industrial applications due to their simple heat treatment based on the solid-state reaction synthesis using MgO and SiO_2 compounds as precursors [25, 26]. Generally, the solid-state reaction increases grain growth and aggregate particles agglomeration, leading to a poor sinterability of the forsterite powder [27, 28]. A diversity of composites were residential to progress the physical and mechanical properties, dielectric constant, thermal conductivity, and mechanical presentation of forsterite ceramics [29, 30]. These properties are improved with the addition of magnesium aluminate spinel, alumina, zirconia and mullite [31, 32].

Many studies dealt with the transformation of serpentine and its associated minerals to refractories using a heating process [33, 34, 35, 36]. The aim of the present study is to assess the possibility of using the sheared serpentine - bearing rocks, Um Seleimat area, CED, Egypt, in the production of forsterite and/or spinel bodies. by adding calculated amounts of used magnesia and/or bauxite to convert the low-melting metasilicate serpentine to the high-melting orthosilicate, so improve the physical and thermo-mechanical properties of the fired batch.

2. MATERIALS AND METHODS

2.1 Materials

In this study, three types of materials are used; 1) serpentine - bearing rocks (sheared serpentinized ultramafic rocks) as a raw material, 2) used magnesia bricks powder, and 3) calcined bauxite.

Regarding the first type, it was obtained from Um Seleimat area (Figure-1), south Quft-Qusier asphalt road at central Eastern Desert, Egypt between 25°56` - 26°00` N Lat. and 33°45` - 33°55`E Long. The Um Seleimat sheared serpentinized ultramafic rocks were collected to form representative technical sample of the raw serpentine bearing rock.

Concerning with the used magnesia, it was established from lime kilns of the Egyptian Iron and Steel Company (Helwan, Cairo), while the calcined bauxite was established from Alexandrea company for refractories.

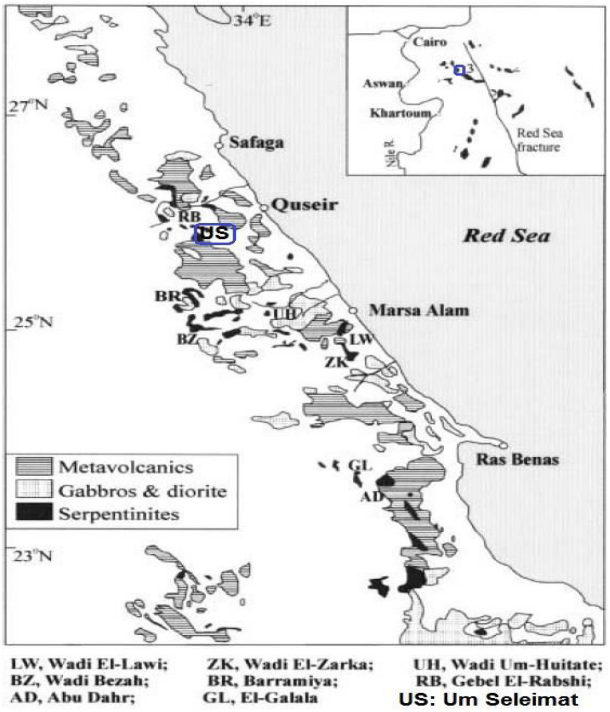

Figure-1. Location map of the study area. Inset the distribution of ophiolitic fragments in ANS [13].

2.2 Methods

2.2.1 Stating materials examination:

The chemical analysis of the starting materials was carried out the National Research Center Laboratories using "XRF" technique (Axios Sequential WD_XRF Spectrometer, Philips-PAnalytical 2005). The ASTM E1621 standard guide for elemental analysis by wave length dispersive X-ray fluorescence spectrometer and the ASTM D7348 standard test method for loss on ignition (LOI) of solid combustion were used as guideline. The mineralogical analysis was performed using X-ray diffraction analysis (XRD) (Philips X-ray diffractometer, Mod. PW 1390 with Ni-filtered Cu-K d radiation).

2.2.2 Batch preparation

The natural material (sheared serpentinized ultramafic rocks), in addition to used magnesia and calcined bauxite, were crushed in a jaw crusher and finely ground in a pilot plant steel ball mill to reach 90 µ. Two batches were prepared to produce the forsterite and spinel forsterite composites. The ground materials were mixed with 2% PVA solution, to a semi-dry state, and then pressed under 60kg/cm^2 load using one-inch square mould. The shaped briquettes were dried at 110° C over night and fired at 1500°C for 2-hour using one stage firing process technique.

2.2.3 Batch testing

Several analyses were carried out to study and assess the prepared samples such as XRD, FTIR and SEM techniques. The chemical analysis, morphology and the microstructure investigation of the samples were carried

out using SEM (Model Quanta FEG250, coupled with energy-dispersive spectroscopy EDAX). The bond vibration of the radical groups was tested using FTIR (absorption spectra by Elmer-783 double-beam dispersion spectrophotometer using standard KBr). 300 mg KBr were homogenized with 2 mg of the sample in a vibration mill, evacuated, and the tablets were pressed for 5 minutes under pressure of 10 MPa. The recording time was 20 minutes and the range 4000 - 400 cm^{-1}.

The solid stage composition as well as the microstructure and microchemistry of the batches were approved using XRD and SEM as with EDAX techniques, respectively.

The densification parameters of the fired briquettes in terms of bulk obvious density and porosity were determined according to kerosene displacement method. Refractoriness under load and thermal shock resistance tests were carried out to show the maximum temperature and number of heating cycles respectively, at which the samples could bear. In addition, the compressive strength test of the fired batches was conducted to show the maximum load they could bear.

3. RESULTS AND DISCUSSIONS

3.1 Geological setting

The Um Seleimat serpentinite rocks are about 15 km long, NW-SE trend, and are found in sharp and distinct contact with adjacent basement rocks [37,38].The serpentinite represents the originally elongated along NW-SE brittle-ductile shear zones of Um Seleimat area and form up to 27% of the total area (Figure-2). Serpentinites are genetically and spatially associated with the sequences of ultramafic to maficrocks. Hume 1925 [39] recognized the existence of mafic-ultramafic bodies and noticed its widely distributed in the central and southern parts of the Eastern Desert. In 1958 the term ophiolite sequence has been used to describe the large masses of ultramafic to maficrocks that including serpentiniteat Barramiya [40]. Later many authors [41, 13, 14, 42], recognized and characterized some of the Pan African mafic- ultramafic serpentinitebodies as ophiolites, that are widely scattered in the CED of Egypt as a part of the Neoproterozoic ANS. The ANS represents the Neoproterozoic Pan African crust formed between 900-550 Ma [15, 43]. Ali Bik *et al*, 2017 [44], assigned the Sa'al complex as the oldest arc rocks of the ANS (pre- Pan African?), that expanded the ANS tectonomagmatic stages from late Mesoproterozoic to late Neoproterozoic (?). The ophiolite sequences of Egypt are typically dismembered and form allochthonous bodies of ophiolitic serpentinites and associated sub-ophiolitic metamorphic sole(amphibolites), formed in afore-arc/arc/back-arc system above SE- and NE-dipping supra-subduction zones [45, 42]. Serpentinites generally form elongated ranges defining folded tabular bodies or sheets and formed as obducted slices of oceanic lithosphere emplaced onto the island arc succession [14, 16, 17, 21]. Two varieties of serpentinites are distinguishable among ophiolitic mélange of Egypt, namely, massive and sheared serpentinites [17, 18, 20, 21]. In um seliemat both of the massive and sheared serpentinites are present (Figure-3), the massive one highly mining for its ornamental characters, while the sheared one is useless because it's highly fractures and increasing the iron content.

3.2 Assessment of the starting materials

Besid serpentines, the raw materials including both of used magnesia bricks powder and calcined bauxite. The chemical composition of the start materials is displayed in Table-1. It is showed that serpentinite area is mainly composed of hydrated magnesium silicate with substantial amount of iron; the amounts of SiO_2, MgO, FeO and Loss on ignition are 40.55, 37.66, 10.55 and 7.50%, respectively. Slight amount of alumina and titanium oxide are recorded as 1.17 and 0.05%. Minor and

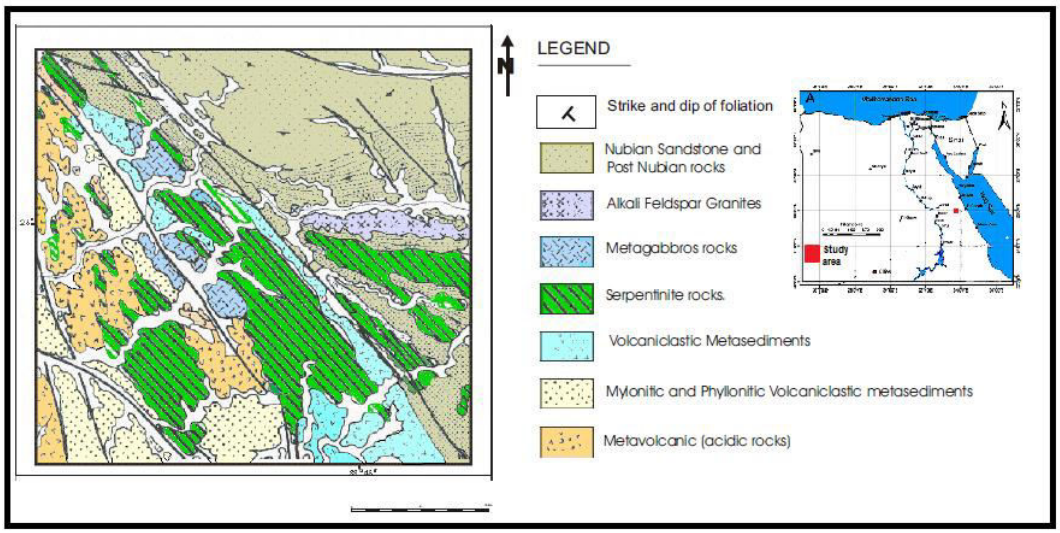

Figure-2. Geological map of the study area [38].

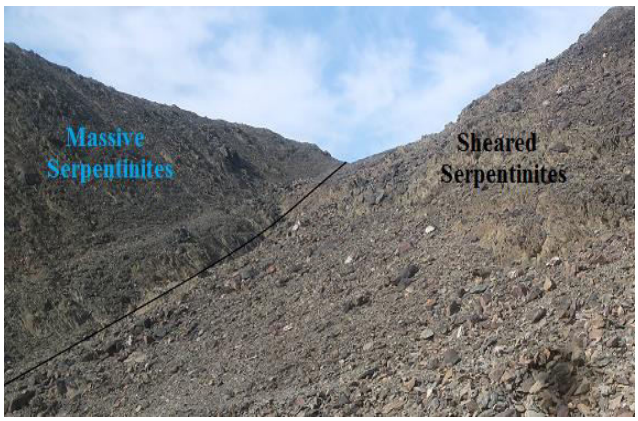

Figure-3. Um Seliemat serpentinite rocks exhibiting massive and sheared types.

Table-1. Chemical composition of the starting materials.

Constituents %	Serpentinite bearing rock	Used magnesia	Calcined bauxite
SiO_2	40.55	1.58	8.49
TiO_2	0.05	-	-
Al_2O_3	1.17	0.67	87.36
Fe_2O_3	10.55	1.66	0.06
MnO	0.18	0.02	-
MgO	37.66	93.23	3.22
CaO	0.78	1.84	0.12
Na_2O	0.05	-	0.23
K_2O	0.02	-	-
P_2O_5	0.24	-	0.05
SO_3	0.08	-	
Cl	0.04	0.02	0.03
Cr_2O_3	0.32	-	-
Co_3O_4	0.03	-	-
NiO	0.72	-	-
ZnO	0.02	-	-
L.O.I	7.50	0.61	0.02
Total	99.96	99.63	99.58

trace amounts of other impurities not exceed 2%, while the chemical composition of the used magnesia confirms that MgO is the main oxide (93.23%), CaO is 1.84%, While Al_2O_3 and Fe_2O_3 are0.67% and 1.66%, respectively. minor amount of loss on ignition is detected as 0.61%. Chemical composition of calcined bauxite shows that it is mainly aluminum oxide (87.36%) beside silica (8.49%) and magnesia (3.22%).

Geochemicaly, whatever the protolith or parent rock is, the studied serpentinites plot in the Alpine-type ultramafic rocks on the Cr2O3-NiO diagram (Figure-4a), implying their exclusive ophiolitic nature. Al2O3- and TiO2-poor matched with S-M-F diagram (Figure-4b), that assign a dunite/peridotite not pyroxenite protolith, what match with the majority of serpentinites in the Eastern Desert of Egypt [13, 14].

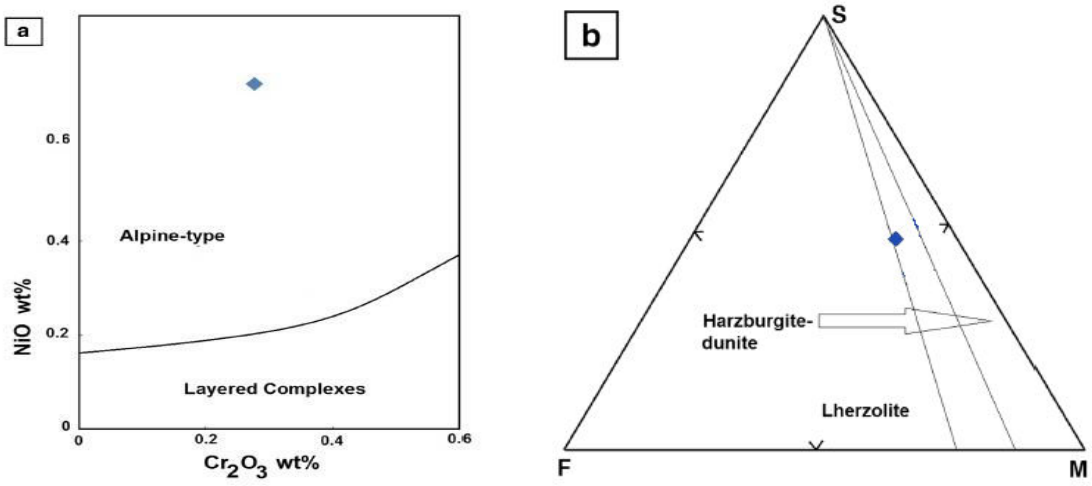

Figure-4. Ophiolitic nature of the Um Seliemat serpentinite based on their whole rock composition.
a; Cr2O3 vs. NiO binary diagram of Irvine and Findlay, 1972 [46].
b; SFM ternary diagram of Pfeifer, 1979[47], where S = SiO2 + Al2O3 + Na2O,
F = FeO + CaO + Al2O3 + 2Na2O and M = MgO + CaO + Al2O3 + 2Na2O.

The serpentinites bearing rock shows that it is massive, hard and their colour is greyish green. Mineral composition of the serpentinites bearing rock carried out by XRD technique confirms that Antigorite mineral is the major mineral with less amount of forsterite mineral (Figure-5).

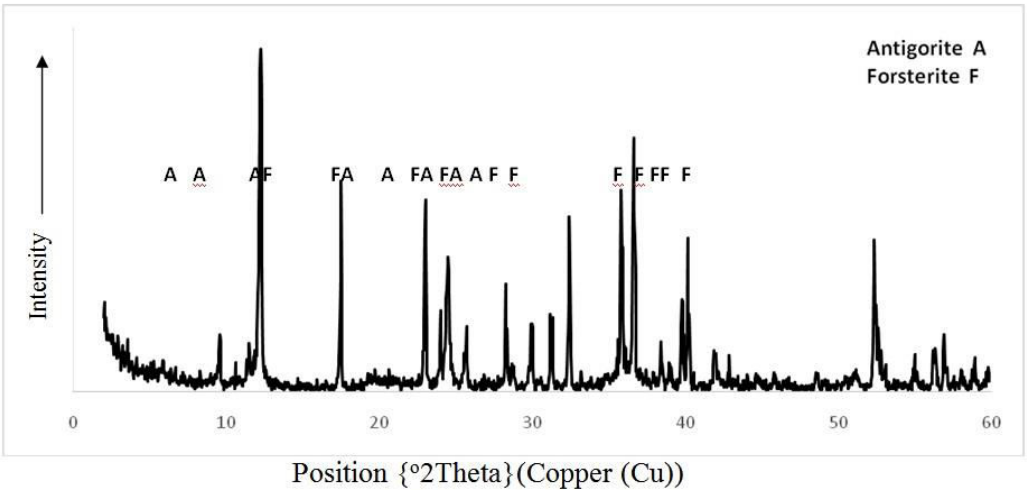

Figure-5. XRD pattern of serpentinite bearing rocks.

Micrographically, serpentine composed of mainly antigorite and olivine with subordinate amount of opaques mainly iron oxides (Figure-6), in some places antigorite shows at margins of olivine crystal as fibro-lamellar structure to indicate come after olivine and olivine crystals are generally consisting of forsterite mainly embedded in serpentinies matrix figure, these textures may give the origin or genesis of serpentinites.

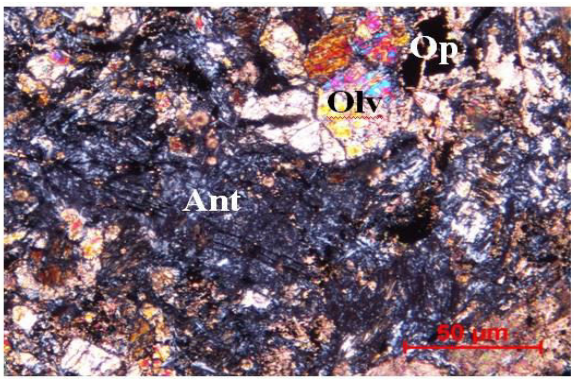

Figure-6. Photomicrograph of the antigorite (Ant) fibro-lamellar showing relics black opaque minerals (Op)and framboidal olivine (OLV) scattered in matrixs.

Solid phase composition of the magnesia that used were performed by XRD confirms that the main phase composition is periclase in addition to the very small amount of CMS phase (Figure-7).

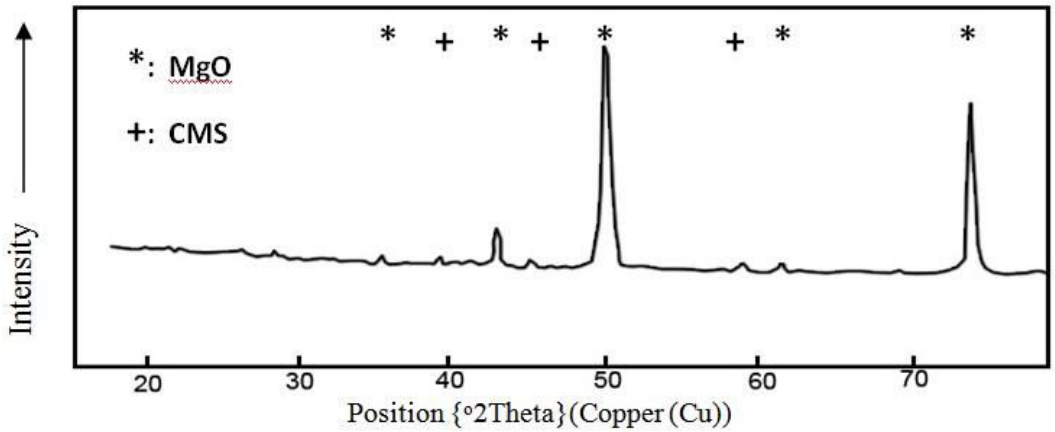

Figure-7. XRD pattern of the used magnesia materials.

Figure-8 illustrate the phase composition of the calcined bauxite, it shows the main phases recorded are corundum and silliminite with qualitative concentration as 80 and 20%, respectively.

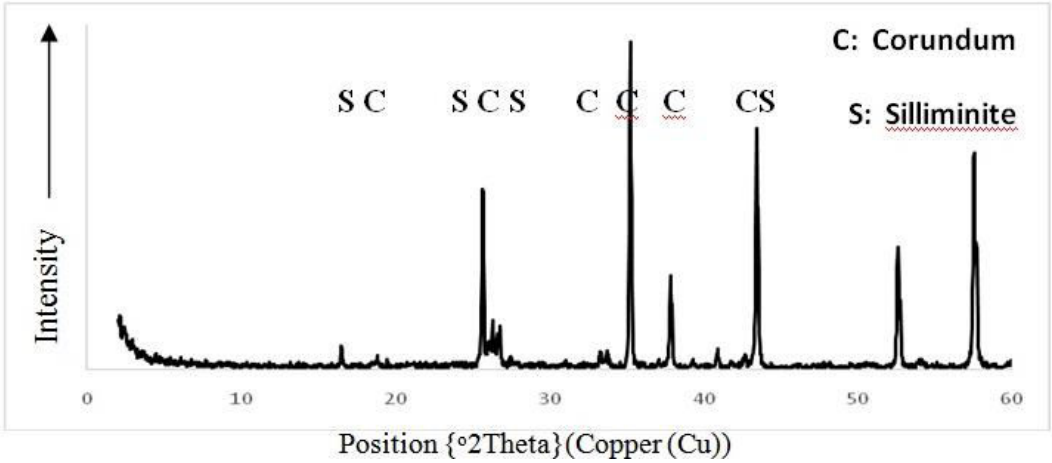

Figure-8. Phase composition of the calcined bauxite.

3.3. Batch calculation

According to the stoichiometry composition of serpentine and forsterite, the serpentine, Mg3SiO5 (OH)4, the amount of MgO is 43.48%, SiO2 is 43.48% and H2O is 4.50 %. whilst the percentage of MgO and silica in forsterite (2MgO. SiO2) are 57.14 and 42.86%, respectively. Thus, significant amount of used magnesia must be added to the serpentinite bearing rock to increase the magnesia in the batch then fired for forming the forsterite refractory mineral. Calculated amounts of serpentinites with used magnesia and / or calcined bauxite were mixed to yield forsterite and/or spinel forsterite, Tables (2 & 3).

Table-2. Batch no. 1, calculated stoichiometry composition of forsterite composites.

Constituents %	Serpentinite bearing rock 100 gm	Used magnesia 20 gm	Total oxides	On calcined basis 100%
SiO_2	40.55	0.32	40.87	36.41
TiO_2	0.30	-	0.3	0.27
Al_2O_3	0.80	0.13	0.93	0.83
Fe_2O_3	10.55	0.33	10.88	9.69
MnO	0.18	-	0.18	0.16
MgO	37.66	18.65	56.31	50.16
CaO	0.78	0.37	1.15	1.02
Na_2O	0.05	-	0.05	0.04
K_2O	0.02	-	0.02	0.02
P_2O_5	0.24	-	0.24	0.21
SO_3	0.08	-	0.08	0.07
Cl	0.04	-	0.04	0.04
Cr_2O_3	0.32	-	0.32	0.28
Co_3O_4	0.03	-	0.03	0.03
NiO	0.72	-	0.72	0.64
ZnO	0.02	-	0.02	0.02
L.O.I	7.50	0.12	7.62	
Total	99.96	19.92	119.88	99.89

Table-3. Batch no. 2, calculated stoichiometry composition of spinel forsterite composite.

Constituents %	Serpentinite bearing rock 100 gm	Used magnesite 30 gm	Calcined bauxite 10 gm	Total oxides	On calcined basis 100%
SiO_2	40.55	0.47	0.85	41.87	31.7
TiO_2	0.30	-	-	0.3	0.23
Al_2O_3	0.80	0.2	8.74	9.74	7.38
Fe_2O_3	10.55	0.5	0.01	11.06	8.38
MnO	0.18	-	-	0.18	0.14
MgO	37.66	27.97	0.322	65.95	49.97
CaO	0.78	0.55	0.012	1.34	1.02
Na_2O	0.05	-	0.023	0.07	0.05
K_2O	0.02	-	-	0.02	0.02
P_2O_5	0.24	-	0.005	0.25	0.19
SO_3	0.08	-	-	0.08	0.06
Cl	0.04	-	0.003	0.04	0.03
Cr_2O_3	0.32	-	-	0.32	0.24
Co_3O_4	0.03	-	-	0.03	0.02
NiO	0.72	-	-	0.72	0.55
ZnO	0.02	-	-	0.02	0.01
L.O.I	7.50	0.18	0.002	7.69	
Total	99.96	29.87	9.957	139.68	99.99

Tables (2 & 3) shows the calculated stoichiometry composition of forsterite mixture from serpentinite and used magnesite. 100 gm of serpentinite added to 20 gm of used magnesia were mixed to give percentage of SiO2 and MgOon calcined basis 36.41 and 50.16%, for batch no.1, then 31.7and 49.97for batch no.2 respectively. These ratios are blocked to the stoichiometry composition of forsterite. Percentage of Fe2O3 and Al2O3 are reacting with the excess magnesia to form magnesia Fe2O3 spinel in the absence of alumina and magnesia, Fe2O3, alumina spinel in the presence of alumina source bauxite.

Each batch was mixed well, then pressed using semi-dry 2% PVA solution and 1 inch square mould at 60kg/cm^2. The shaped briquettes were dried at 110^o Cover night and fired at 1500^{o}C for 2 hour using one stage firing process technique.

3.4 Product assessment

The solid phase composition approved by XRD ensures the stoichiometry composition intended to form these phases. Solid phase composition of the fired batches up to 1500^{o}C for 2 hours is illustrated in Figure-9 Forsterite is the major phase recorded in the both batches, while iron rich spinel in detected in batch no. 1 before adding the calcined bauxite. Alumina, Fe_2O_3, magnesia spinel is shown in the second batch after adding the calcined bauxite to increase the alumina percent, which contribute in formation of magnesia-alumina spinel with the periclase.

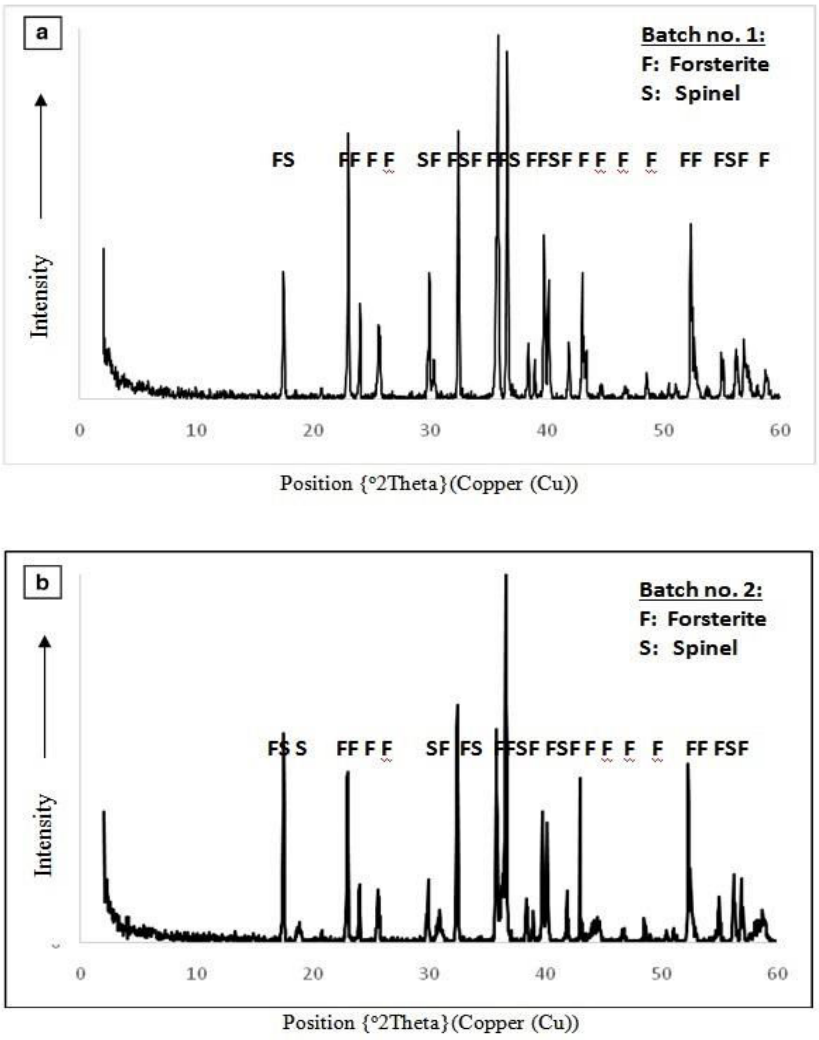

Figure-9. XRD pattern of products fired at 1500^{o}C for 2 hours; a) batch no.1 and b) batch no. 2.

FT-IR techniques investigate bond vibrations of the radical groups, whose spectra absorption bands appear at different frequencies. The band position is compared with the spectra noted in Gadsden, 1975 [48], and possible assignments of the representative spectra for the Um Seliemat serpentinite (S), batch no.1 (B1) and batch no.2 (B2) samples are presented in Figure-10 and Table-4. Absorption bands due to fundamental stretching vibration of hydroxyl groups are observed in the spectral region 3100-3700 cm^{-1} in the IR spectra of the serpentine S sample. This region represented two characterized segments. 1st interlayer water band region recorded at

3100-3560, represented very broad signal in sample S, but sample B1 and B2 shown a weak to absence signal reveal the result of firing process. 2nd hydroxyl of serpentine at 3675, in S sample shown sharp signal and totally disappear in both of B1 and B2 samples due to the firing. Water bending replaced the organic matter to interpret the recorded bands at 1600-1645 cm^{-1} and 2850-2980 cm^{-1}, that not only reveal hydroxyl group of the samples but may also refer to moisture absorption from lab environment and absorption of water molecules from atmospheric air while recording the spectra. Si-O silicates; recorded bands of the main Si-O symmetrical stretching vibration silicate region at 975-1160 (with 1008 peak) in sample S. Due to firing, the silicate stretching band beak of B1 and B2 shifted according to forsterite tetrahedral Si.O4vibration, which represented a gentle wider broad in B1 sample (800-1150) more than B2 sample, which has steep flanks on both sides. The wide gentle broad Si-O4 absorption band of B1 sample may reveal the homogeneity of the mineralogical structure, what mean a complete firing effect led to totally transform of batch 1 to forsterite. On the other hand the sharpen of B2 may be due to the complexity of forsterite/spinel structure. Other Si-O symmetrical stretching vibration silicate band at 777-783 was insignificant in all samples. The main silicate symmetrical bending vibration silicate recorded at 670 represented slightly beak in both B1 and B2 samples, S sample have more beak characterization with shifted signal recorded at 615. The main Si-O asymmetrical bending vibration silicate band at 455-460, was insignificant in all samples. Also the other Si-O asymmetrical bending vibration silicate band at 530-540 was insignificant in all samples. There are three magnesia vibration bands according to bearing minerals; magnesia serpentine Mg-O out of plain vibration band recorded at 545-575 in sample S. Magnesia forsterite octahedral Mg.O6 vibration band recorded at 475 in sample B1. Magnesia spinel vibration band recorded at 525-660 in sample B2.

The microstructure and microchemistry of the fired batches no.1 and no. 2 were detected by using SEM and EDAX as shown in Figures 11 & 12, respectively, both batches shows dissimilar grain size range from fine, medium and coarse of interlocked grains gray and white in colour. High quantity of pore is noticed among the grains in the groundmass, which confirm the low porosity and high the density. Two forms of crystals are recorded, grey type with prismatic and cubic shape in cubic form and bright white in addition to irregular forms of liquid phase. Point analysis no. 1 demonstrates the chemical analysis of the grey phase of prismatic crystal and confirm that this phase is forsterite, which is the main phase recorded by XRD. While point analysis no. 2 indicates that the bright cubic crystals are ferric and alumina magnesia spinel, which was confirmed by the XRD technique as the second major phase in the two batches after the forsterite. Point analysis no. 3 refers to the liquid phase composed of calcium, magnesium, aluminium and iron silicate solid solution, which is responsible for the adhering the main phases together in the sample.

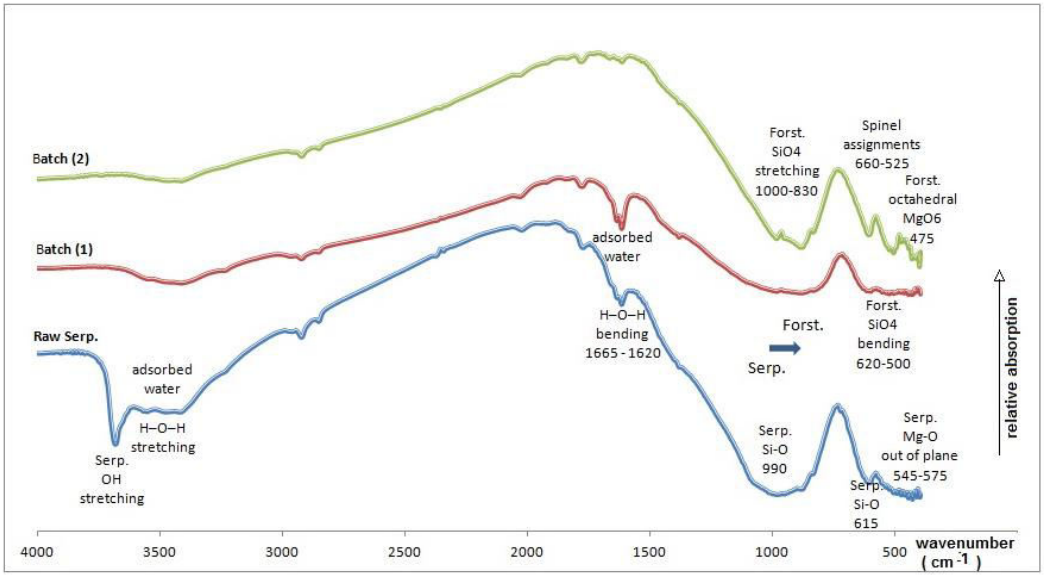

Figure-10. FTIR spectra recorded for raw serpentine, batch no.1 and batch no.2.

Table-4. FT-IR spectra absorption bands of bond vibrations.

Band Frequency wave number (cm^{-1})	Band Assignments	Remarks
455-460	Si-O, asymmetrical bending vibration	insignificant
475	Octahedral Mg.O vibration	B2 (narrow sharp)
530-540	Si-O, asym. bending vibration	insignificant
545-575	Mg-O out of plain (serpnt.)	S (remarkable)
525-660	Mg. Spinel assignments	B2 (narrow sharp)
615	Si-O, symmetrical bending vibration	S (remarkable)
500-620	Si.O4, tetrahedral bending vibration	B1 (wide broad)
670-695	Si-O, sym. bending vibration	B1, B2
777-783	Si-O, sym. stretching vibration	insignificant
975-1160 (1008)	Si-O, sym. stretching vibration	S (remarkable)
830-1000	Si.O4, tetrahedral bending vibration	B2 (narrow sharp)
800-1150	Si.O4, tetrahedral bending vibration	B1 (wide broad)
1600-1645	Absorbed water bending, serpent./moisture	S (remarkable) / meaningless due to moisture
2850-2980	Absorbed moisture water replaced the organics	meaningless due to moisture
3100-3560	Interlayer water stretching	S broad signal with steps remarkable flank
3675	OH^- stretching vibration of serpentine	S (sharp)

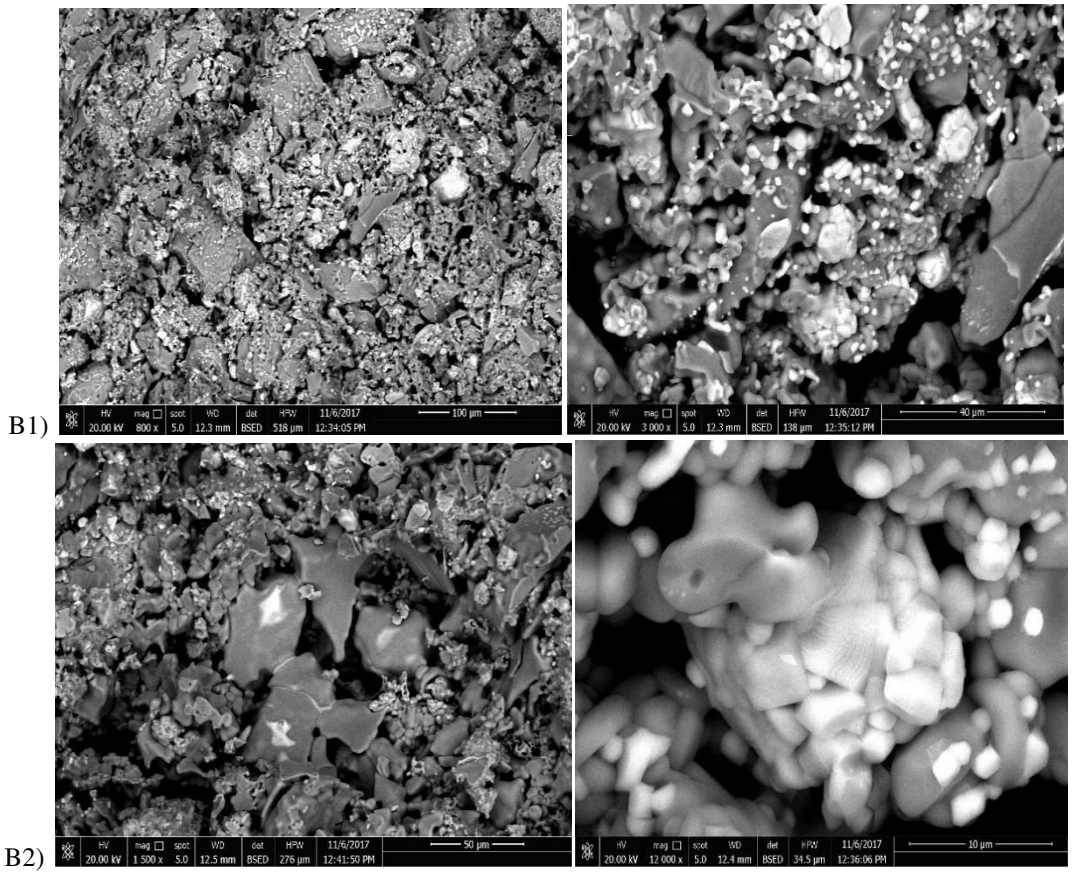

Figure-11. SEM of the prepared batches no.1 (B1) andno.2 (B2) fired at $1500^{O}C$ for 2 hours.

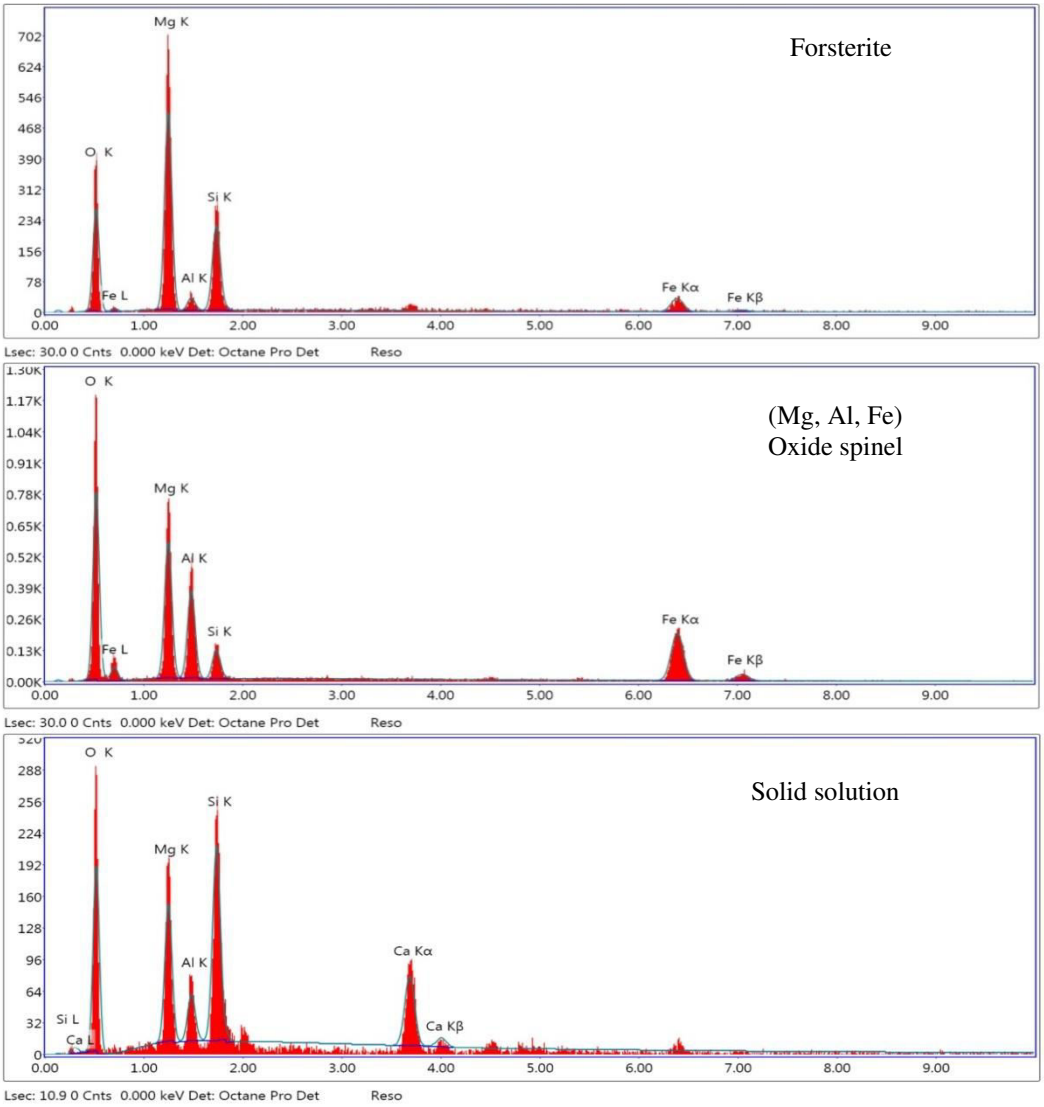

Figure-12. EDAX analysis of the prepared batches fired at 1500^{O}C for 2 hours.

Densification properties of the fired batches illustrate in Table-4. Bulk density of batch no. 1 shows 2.35g/cm^3, while that of the second batch is 2.40g/cm^3, respectively. Obvious porosity has an overturn relation to the bulk density and the linear shrinkage. The apparent porosity of the forsterite batch is 28.60%, while these of periclase forsterite 27.60%, respectively.

Table-5. Densification parameters of the fired batches at 1500oC for 2 hours.

Batch no.	Bulk density g/cm^3	Apparent porosity %	Linear shrinkage	CCS Kg/cm^2	Ta ^{o}C	Thermal shock resistance (no. of cycles)
1	2.35	28.60	+0.49	191	1400	>10
2	2.40	27.60	+0.34	247	1420	>10

Linear shrinkage of the two batches record positive results, it increases in the batch no. 1 and shows +0.49% with slightly decreasing to +0.34% in batch no. 2. This is due to the slightly liquid phase formation in the second batch more than the first one.

Compressive strength of the fired batches based mainly of the densification properties of the fired batches as well as their mineral constitution and the liquid phase formed. Batch no. 1 shows lower density and shrinkage as well as higher porosity. So it shows lower compressive strength than the second batch as illustrated in Table-5. The compressive strength recorded for the batch no.1 is 191kg/cm^2, while that of the second one is 247kg/cm^2, respectively. This is due to the high liquid phase content in the second batch more than the first one.

Thermal shock resistant represented by the number of heating and cooling cycles is illustrated in Table-5. It is noticed that it is record more than ten heating and cooling cycles for both of the two batches.

Refractoriness under load of the fired batches is performed for the wished-for batches fired at 1500°C for 2 hours to detect the thermal behavior and the maximum working temperature for each one (Figure-13). The refractoriness cost depends on the chemical and firing temperature, phase composition, phases formed after firing at 1500°C in addition to the liquid phase. Under load of 2kg/cm^{2}the maximum bearing temperature (Ta) for the the first batch, with addition of used magnesia, is 1400°C, while the second batch, after additing of used magnesia and bauxite is 1420°C. This mainly due to the additional bauxite with the used magnesia leads to slightly improve the refractory quality due to the formation of alumina, ferric spinel refractory phases compared to the ferric spinel refractory phase. This shows that the addition of magnesia and bauxite improves the refractory quality of the forsterite ceramic material.

These ceramics material are suggested to apply in lining of permanent steel ladles and layer of iron as well as the brick network in the heat exchangers of glass furnaces.

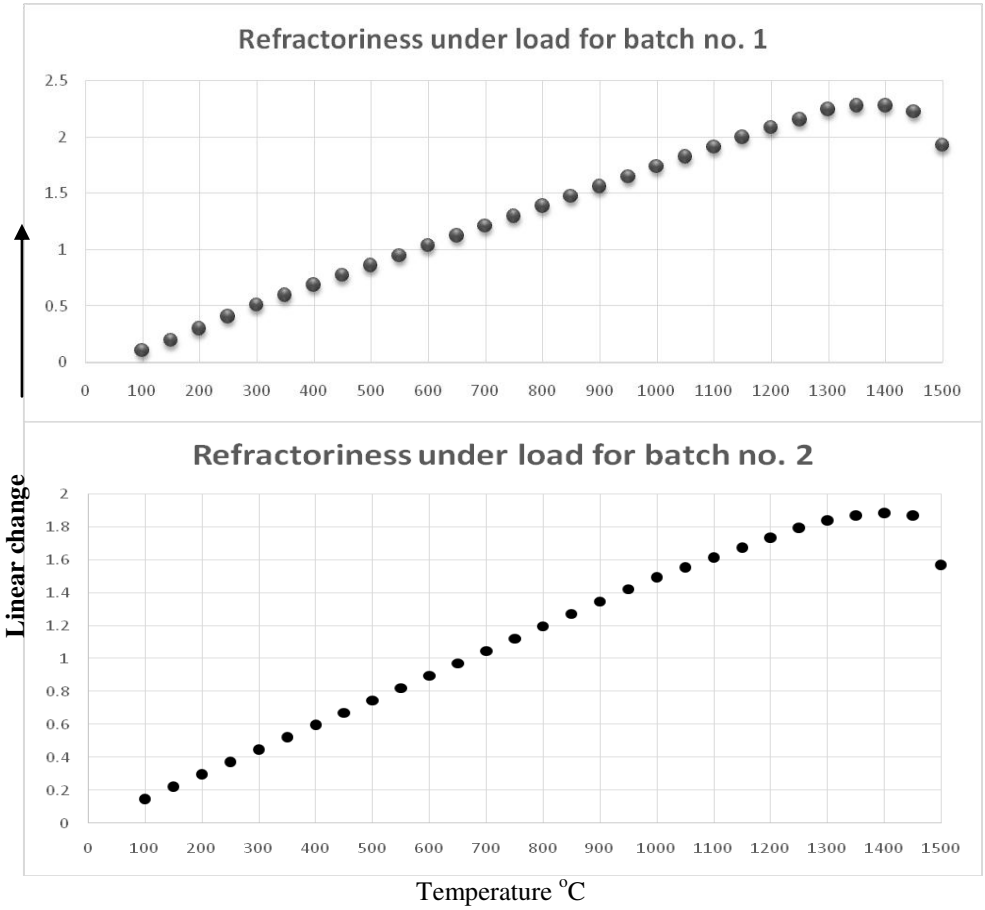

Figure-13. Refractoriness under load of the prepared batches fired at 1500°C for 2 hours.

CONCLUSIONS

- Two batches composed of serpentinites bearing rocks as well as used magnesite and/or bauxite are designed to synthesis forsterite and/or spinel forsterite refractory phases.
- Chemical and mineral compositions of the starting materials were carried out.
- The microstructure and phase composition of the fired batches at 1500oC for 2 hours confirm that forsterite and spinel refractory phases are formed.
- Densification properties show that the bulk densities of these batches are 2.35 and2.40g/cm3, respectively. While their porosities are 28.60and27.60 % and shrinkage +0.49 and +0.34% respectively
- Compressive strength of the two batches is increased by increasing the liquid phase from batch no. 1 as 191kg/cm2 to batch no. 2 as 247kg/cm2.
- Refractoriness under load confirms that the addition of bauxite improves the refractoriness of the batch from 1400oC in batch no. 1 to 1420oC in batch no. 2
- Good thermo-mechanical results are recorded for the two batches.
- These refractory bodies are recommended applying in lining of permanent layer of iron and steel ladles and the brick network in the heat exchangers of glass furnaces.

REFERENCES

[1] Birch R. E. & Harvey F. A. 1935. Forsterite and other magnesium silicates as refractories. J. Am. Ceram. Soc. 18, 176-192.

[2] Li J., Zhang Y., Shao S., Zhang S. & Ma S. 2016. Application of cleaner production in a Chinese magnesia refractory material plant. J. Clean. Prod. 113, 1015-1023.

[3] Carniglia S. & Barna G. 1992. Foundations of Refractory Application. Handbook of Industrial Refractories Technology - Principles, Types, Properties and Applications.

[4] Schacht C. 2004. a. (Org. Refractories Handbook. Mechanical Engineering. doi:10.1017/CBO9781107415324.004

[5] Horai K. & Simmons G. 1969. Thermal conductivity of rock-forming minerals. Earth Planet. Sci. Lett. 6, 359-368.

[6] Deer W. A., Howie R. A. & Zussman J. 1986. Rock-Forming Minerals. Disilicates and Ring Silicates1B.

[7] Deer W. A., Howie R. A. & Zussman J. 1992. An introduction to the rock-forming minerals. Second edition. An introduction to the rock-forming minerals. Second edition.

[8] Wood B. J. & Kleppa O. J. 1981. Thermo chemistry of forsterite-fayalite olivine solutions. Geochim. Cosmochim. Acta. 45, 529-534.

[9] Martin B. & Fyfe W. S. 1970. Some experimental and theoretical observations on the kinetics of hydration reactions with particular reference to serpentinization. Chem. Geol. 6, 185-202.

[10] Wegner W. W. & Ernst W. G. 1983. Experimentally determined hydration and dehydration reaction rates in the system MgO-SiO2-H2O. Am. J. Sci. 283, 151-180.

[11] Malvoisin B., Brunet F., Carlut J., Rouméjon S. & Cannat M. 2012. Serpentinization of oceanic peridotites: 2. Kinetics and processes of San Carlos olivine hydrothermal alteration. J. Geophys. Res. Solid Earth. 117.

[12] Beard J. S. *et al*. 2009. Onset and progression of serpentinization and magnetite formation in Olivine-rich troctolite from IODP hole U1309D. J. Petrol. 50, 387-403.

[13] Shackleton R. M., Ries A. C., Graham R. H. & Fitches W. R. 1980. Late Precambrian ophiolitic melange in the Eastern Desert of Egypt. Nature. 285, 472.

[14] Ries A. C., Shackleton R. M., Graham R. H. & Fitches W. R. 1983. Pan-African structures, ophiolites and mélange in the Eastem Desert of Egypt: a traverse at 26 N. J. Geol. Soc. London. 140, 75-95.

[15] Stern R. J. 1994. Arc assembly and continental collision in the Neoproterozoic East African Orogen: implications for the consolidation of Gondwanaland. Annu. Rev. Earth Planet. Sci. 22, 319-351.

[16] Stern R. J., Johnson P. R., Kröner A. & Yibas B. 2004. Neoproterozoic ophiolites of the Arabian-Nubian shield. Dev. Precambrian Geol. 13, 95-128.

[17] Ali-Bik M. W., Taman Z., El Kalioubi B. & Abdel Wahab W. 2012. Serpentinite-hosted talc-magnesite deposits of Wadi Barramiya area, Eastern Desert, Egypt: Characteristics, petrogenesis and evolution. J. African Earth Sci. doi: 10.1016/j.jafrearsci.2011.11.002

[18] Ali-Bik M. W., Abd El Rahim S. H. & Wahab W. A. 2014. Hornblende gabbros of Wadi Az Zarib area, Central Eastern Desert, Egypt: opaque mineralogy, geochemistry, tectonic setting, and petrogenesis. Arab. J. Geosci. 7.

[19] Surour A. A. 2017. Chemistry of serpentine “polymorphs” in the Pan-African serpentinites from the Eastern Desert of Egypt, with an emphasis on the effect of superimposed thermal metamorphism. Mineral. Petrol. 111, 99-119.

[20] Khalil A.E., El-Desoky H.M., Shahin T.M. & Abdelwahab W. 2018. Late Cryogenian arc-related volcaniclastic metasediment successions at Wadi Hammuda, Central Eastern Desert, Egypt: geology and geochemistry. Arab. J. Geosci. 11: 74.

[21] Ali-Bik M. W. *et al*. 2018. The late Neoproterozoic Pan-African low-grade metamorphic ophiolitic and island-arc assemblages at Gebel Zabara area, Central Eastern Desert, Egypt: Petrogenesis and remote sensing - Based geologic mapping. J. African Earth Sci. 144, 17-40.

[22] Ahmed A. H., Gharib M. E. & Arai S. 2012. Characterization of the thermally metamorphosed mantle-crust transition zone of the Neoproterozoic ophiolite at Gebel Mudarjaj, south Eastern Desert, Egypt. Lithos. 142-143, 67-83.

[23] Khalil N. M., Hassan M. B., Ewais E. M. M. & Saleh F. A. 2010. Sintering, mechanical and refractory properties of MA spinel prepared via co-precipitation and sol-gel techniques. J. Alloys Compd. 496, 600-607.

[24] Mitchell M. B. D., Jackson D. & James P. F. 1998. Preparation and characterisation of forsterite (Mg2SiO4) aerogels. J. Non. Cryst. Solids. 225, 125-129.

[25] Mustafa E., Khalil N. & Gamal A. 2002. Sintering and microstructure of spinel-forsterite bodies. Ceram. Int. 28, 663-667.

[26] Othman A. G. M. & Khalil N. M. 2005. Sintering of magnesia refractories through the formation of periclase-forsterite-spinel phases. Ceram. Int. 31, 1117-1121.

[27] Brindley G. W. & Hayami R. 1965. Kinetics and mechanism of formation of forsterite (Mg2SiO4) by solid state reaction of MgO and SiO2. Philos. Mag. 12, 505-514.

[28] Szczerba J., Pedzich Z., Nikiel M. & Kapuścińska D. 2007. Influence of raw materials morphology on properties of magnesia-spinel refractories. J. Eur. Ceram. Soc. 27, 1683-1689.

[29] Kawamoto T. *et al*. 2004. Mg/Si ratios of aqueous fluids coexisting with forsterite and enstatite based on the phase relations in the Mg2SiO4-SiO2-H2O system. Am. Mineral. 89, 1433-1437.

[30] Tsunooka T., Androu M., Higashida Y., Sugiura H. & Ohsato H. 2003. Effects of TiO2on sinterability and dielectric properties of high-Q forsterite ceramics. J. Eur. Ceram. Soc. 23, 2573-2578.

[31] Finkelstein G. J. *et al.* 2014. Phase transitions and equation of state of forsterite to 90 GPa from single-crystal X-ray diffraction and molecular modeling. Am. Mineral. 99, 35-43.

[32] Braulio M. A. L., Brant P. O. C., Bittencourt L. R. M. & Pandolfelli V. C. 2009. Microsilica or MgO grain size: Which one mostly affects the in situ spinel refractory castable expansion? Ceram. Int. 35, 3327-3334.

[33] BnTNDLEv G. W. and Zussuax J. 1957. A Structural study of the thermal transformation of serpentine minerals to Forsterite. TIIE Am. Mineral. 42, 461-474.

[34] Elmaghraby M. S., Ismail A. I. M., Abd El Ghaffar N. I. 2015. Atalla Egyptian Serpentinite for Producing Forsterite and its Thermo-Mechanical Behavior. Int. J. Res. Stud. Sci. Eng. Technol. 2, 137-146.

[35] Serry M. A., Ahmed S. E., Ali Bik M. W. & Abdel Wahab W. 2011. Assessment of Egyptian talc-carbonate deposits in production of shaped cordierite-ceramics for thermo-mechanical applications. CFI Ceram. Forum Int.

[36] Cheng T. W., Ding Y. C. & Chiu J. P. 2002. A study of synthetic forsterite refractory materials using waste serpentine cutting. Miner. Eng. 15, 271-275.

[37] Noweir A. M. 1968. Geology of the Hammamat-Um Seleimat district, Eastern Desert, Egypt. Unpubl. PhD thesis, Assuit Univ. Egypt.

[38] Akaad M. K. & Noweir A. M. 1969. Lithostratigraphy of the Hammamat-Um Seleimat District, Eastern Desert, Egypt. Nature. 223, 284.

[39] Hume W. F. 1925. Geology of Egypt, vol. I. Surv. Egypt, Le Caire.

[40] Rittmann A. 1958. Geosynclinal volcanism, ophiolites and Barramiya rocks. Egypt J. Geol. 2, 61-66.

[41] El Sharkawy M. A. & El Bayoumi R. M. 1979. The ophiolites of Wadi Ghadir area, Eastern Desert, Egypt. Ann. Geol. Surv. Egypt. 9, 125-135.

[42] Khedr M. Z. & Arai S. 2013. Origin of Neoproterozoic ophiolitic peridotites in south Eastern Desert, Egypt, constrained from primary mantle mineral chemistry. Mineral. Petrol. 107, 807-828.

[43] Ali K. A. *et al*. 2010. Age constraints on the formation and emplacement of Neoproterozoic ophiolites along the Allaqi - Heiani Suture, South Eastern Desert of Egypt. Gondwana Res. doi:10.1016/j.gr.2010.03.002

[44] Ali-Bik M. W., Abd El Rahim S. H., Wahab W. A., Abayazeed S. D. & Hassan S. M. 2017. Geochemical constraints on the oldest arc rocks of the Arabian-

Nubian Shield: The late Mesoproterozoic to late Neoproterozoic (?) Sa'al volcano-sedimentary complex, Sinai, Egypt. Lithos. 284-285.

[45] Farahat E. S. 2011. Geotectonic significance of Neoproterozoic amphibolites from the Central Eastern Desert of Egypt: A possible dismembered sub-ophiolitic metamorphic sole. Lithos. 125, 781-794.

[46] Irvine T. N. & Findlay T. C. 1972. Alpine-type peridotite with particular reference to the Bay of Islands igneous complex. Earth Phys. Branch, Dep. Energy, Mines Resour. Publ. 42, 97-140.

[47] Pfeifer H. R. 1979. Fluid-gesteins-interaktion in metamorphen ultramafititen der Zentralalpen.

[48] Gadsden J. A. 1975. Infrared spectra of minerals and related inorganic compounds. (Butterworths).